Interfacing Modular Multilevel Converters for Grid Integration of Renewable Energy Sources

Fatemeh Shahnazian[a], Jafar Adabi[a,*], Edris Pouresmaeil[b,c], and João P. S. Catalão[b,d,e,*]

[a] Faculty of Electrical and Computer Engineering, Babol (Noshirvani) University of Technology, PO Box 484, Babol, Iran
[b] INESC-ID, Instituto Superior Técnico, University of Lisbon, 1049-001 Lisbon, Portugal
[c] Department of Electrical Engineering and Automation, Aalto University, 02150 Espoo, Finland
[d] INESC TEC and Faculty of Engineering of the University of Porto, 4200-465 Porto, Portugal
[e] C-MAST, University of Beira Interior, 6201-001 Covilha, Portugal

Abstract: This paper presents a control method for modular multilevel converters (MMCs) as an interface between renewable energy sources and the grid. With growing penetration of renewable energy sources in the power grid, the developments in converter technologies and controller designs become more prominent. In this regard, dynamic and steady state analysis of the proposed model for an MMC use in a renewable energy based power system are provided through dc, 1st, and 2nd harmonic models of the converter in dq reference frame. This detailed configuration is then used to accomplish converter modulation and controller design. The first novel contribution of this control method is to provide an accurate pulse width modulation (PWM) strategy based on network and converter parameters, in order to achieve a stable operation for the interfaced MMC during connection of renewable energy sources into the power grid. In addition, the proposed method is able to mitigate the converter circulating current by inserting a second harmonic reference in the modulation process of the MMC, which is the second contribution this paper provides over other control techniques. A capacitor voltage balancing algorithm is also included in this control method to adjust each sub-module (SM) voltage within an acceptable range. Finally, converter's maximum stable operation range is determined based on the dynamic equations of the proposed model. The functionality of the proposed control method is demonstrated by detailed mathematical analysis and comprehensive simulations with MATLAB/Simulink.

Keywords: Capacitor voltage balancing; circulating current control; modular multilevel converter (MMC); power system dynamics; renewable energy sources.

1. Introduction

The recent energy plan is mainly focused on substitution of current energy sources with cheaper, cleaner, and renewable ones. Common environmental concerns based on the rapid utilization of high-priced exhaustible sources have led to major alterations in power system design [1]. For several decades, it has been typical to design the structure of power distribution systems radially in order to improve the simplicity of the control system [2]. However, today with rising volatility and unpredictability of the network behavior, creative devices are required to handle such situations successfully. The necessity of designing power networks with maximum power transfer ability and minimum costs leads to the application of power electronics in power system [3]. Development of distributed generation (DG), high voltage direct current transmission systems (HVDC), flexible ac transmission systems (FACTS) and variable-speed drives (VSD) are the main motivation of essential advancements in different power electronic categories such as converter design and

* Corresponding authors: Jafar Adabi (j.adabi@nit.ac.ir) and João P. S. Catalão (catalao@ubi.pt).

switching technology for more than last twenty years [4]. The incessant progress of high voltage and high power switching devices has a great effect on power electronic technology used in power networks [5]. Besides, improved efficiency as well as lower losses and costs make dc collection and transmission systems more beneficial than ac ones [6]. Therefore, power electronic converters are strongly required in this field.

As the most primitive type of converters, output voltage of a 2-level converter has high total harmonic distortion (THD) which necessitates additional massive and expensive ac filters. Also, large number of series-connected switches is required in order to face the high amount of voltage stress [7]. On the contrary, multilevel converters create a stair case voltage waveform consuming capacitors, inductors, or other kinds of separate dc voltage or current sources [5]. This makes multilevel converters widely accepted for industrial applications and high power systems [8] due to reduced voltage stress (dv/dt), lower switching losses and small common-mode voltages, the simplicity of redundancy, and lower filter expenses. Among different multilevel converter topologies proposed for grid connection of renewable energy sources, hybrid multilevel converter structures including series connected three-level neutral point clamped (NPC) converter and H-bridge (HB) modules, the five-level active neutral point converter (ANPC), and series connected five-level ANPC and HB are more common (specially in wind power systems)[9]. As the voltage and power ranges of practical switching devices are limited due to semiconductor technology, series connection of switches is required in case of high voltage and high power operation [10]. This way, the non-modular configuration imposes extra costs and control complexity on the whole system design [5] which limits the voltage level increment of multilevel converters in industrial applications.

To resolve such shortcomings, Marquardt and Lesnicar proposed modular multilevel converter (MMC) in 2003 [11]. Since then, a variety of MMC applications such as HVDC [12], [13] and ac motor drives [14] have been introduced in many papers. Besides this, the converter structure itself can be studied from different aspects. There are several modulation methods some of which are more complex including many details [15], while the others are easier to follow. Space vector [16], nearest level [17], pulse width modulation (PWM) [18], and open loop modulation [19] are such noted examples among them. Comparison of the effects of these methods on various outcomes [20], especially losses [21] could lead to the best choice proportionate to the objective function. In addition, capacitor voltage balancing [22] and circulating current control [23] are two essential control algorithms that should be included in order to achieve stable operation. However, there are other important control objectives such as ac or dc voltage links [24], [25] and converter energy storage capability [26].

Prior to all of the above mentioned features, modeling has a huge impact on any other investigated aspect. Reference [27] represents a single-phase dynamic model of MMC in which sum capacitor voltage of modules in each arm is considered instead of the single module voltages to reduce the complexity of the overall system model.

In order to have more accurate results, a frequency domain approach could be used to compute inner MMC variables [28]. In this method, first, the circuit topology can be divided into dc and ac parts by decoupling the circuit equations through a linear transformation. Then, using iterated convolution, the variables of series-connected modules are calculated in the frequency domain. On the other hand, the simulation of MMC transients especially in integration with large networks becomes complicated as the detailed modeling of converter imposes a massive computational burden on electromagnetic transient-type (EMT-type) programs. In order to find the most efficient and accurate representation of MMC in such cases, different types of models should be developed and compared [29], [30].

This paper presents an analytical dynamic MMC model which is convenient for small signal MMC stability studies and controller design. The studied converter is considered as an interface between a stable dc-link fed from a renewable energy source and distribution power grid. The modeling procedure has been accomplished in dq frame, which is chosen to discuss dynamic state-space equations as it has the advantage of unified control of three-phase over averaging abc models. Thus, generating modulation indices relevant to external demands, as well as internal converter parameters, leads to an accurate control method, being one of the novel contributions this paper provides. A circulating current control algorithm is also designed based on second harmonic equations of the proposed model. Connecting renewable energy sources into the power grid, the detailed dq frame based configuration of the model modulation and control guarantees the stable operation of MMC switches in the determined maximum stable operation range.

The rest of this paper is organized as follows. Section II includes a brief overview of the topology followed by dynamic operation analysis of the proposed model. Section III provides the steady state behavior of MMC connected to a balanced network. Modulation indices also have been calculated using these equations. Circulating current control is investigated in section III-A while capacitor voltage balancing algorithm and converter's stable operation range are discussed in section III-B and section III-C, respectively. The results of this study in section IV are carried out based on time-domain simulations in the MATLAB/Simulink environment, and then followed by some final conclusions in Section V.

2. General System Overview and Dynamic Operation Analysis of the Proposed Model

The electricity produced by renewable energy sources can be transmitted in different forms. Meanwhile, dc transmission systems are more advantageous than ac ones, especially in long distance transmissions where the high expenses for power electronic converters become more cost effective. Increased penetration of such systems due to lower dependence on fossil fuels as well as considerable use of renewable energy sources can lead to the greater importance of fault management and the development of multi-terminal networks. This way, the superior features of MMC will increase the importance of the structure development and controller design.

The general structure of a three phase MMC dc/ac converter under grid-connected operating mode is shown in Fig. 1(a). Each leg is composed of upper and lower arms which consist of N series-connected sub-modules (SM). The most common structure of SMs, as illustrated in Fig. 1(b), are half-bridges wherein IGBT switches are used along with dc capacitors.Besides that, the fault currents as well as harmonic components of arm-currents are limited by two arm inductors, represented by inductance L_{arm}. Parasitic resistances (R_{arm}) vary based on the operational conditions as they indicate inductor resistances and converter losses.

Desired output voltage can be achieved by varying the upper and lower arm voltages which depend on the number of inserted SMs in each arm. Inserted voltages of each upper and lower arm (denoted by *u* and *l* respectively) can be defined as $U_{cux} = n_{ux} U_{cux}^{\Sigma}$ and $U_{clx} = n_{lx} U_{clx}^{\Sigma}$, $x = a,b,c$ where (n_{ux} , n_{lx}) are control modulation indices and (U_{cux}^{Σ} , U_{clx}^{Σ}) represent sum capacitor voltages of each arm. In addition to that, according to Fig. 1(a), the corresponding arm currents i_{ux} and i_{lx} can be expressed as:

$$i_{ux} = i_{circx} + \frac{i_x}{2} \tag{1}$$

$$i_{lx} = i_{circx} - \frac{i_x}{2} \tag{2}$$

where, i_x is the fundamental sine wave current of phase *x* and i_{circx} is the circulating current of leg *x* (which is flowing through dc link and upper and lower arms of each leg). Circulating current consists of dc and second harmonic components and can be given as:

$$i_{circx} = \frac{i_{ux} + i_{lx}}{2} \tag{3}$$

Following that, applying KVL to both upper and lower arms of the MMC structure represented in Fig. 1(a) leads to:

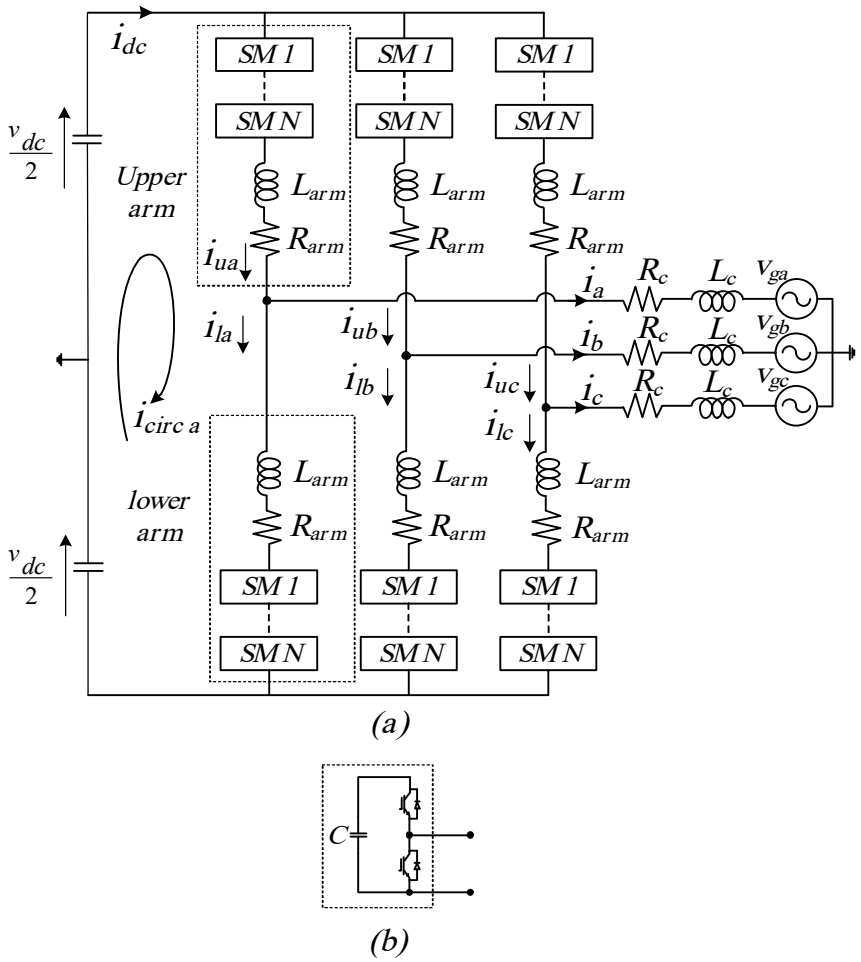

Fig.1.General structure of MMC in grid-connected operating mode, (a) Circuit diagram, (b) SM configuration.

$$n_{ux} U_{cux}^{\Sigma} = \frac{v_{dc}}{2} - v_x - L_{arm} \frac{di_{ux}}{dt} - R_{arm} i_{ux} \tag{4}$$

$$n_{lx} U_{clx}^{\Sigma} = \frac{v_{dc}}{2} + v_x - L_{arm} \frac{di_{lx}}{dt} - R_{arm} i_{lx} \tag{5}$$

where, v_x represents the output voltage of phase x.

As the first step of designing a control method in order to produce an appropriate modulation index, we need to estimate the harmonic components of the modulation indices. In this regard, sum capacitor voltages of each arm (U_{cux}^{Σ} , U_{clx}^{Σ}) in equations (4) and (5) can be estimated by v_{dc} . Besides that, v_x (as the sinusoidal output voltage of the converter) can be written as a sinusoidal coefficient of v_{dc} . Also, the remaining parts in equations (4) and (5) including upper and lower arm currents, add extra second harmonic coefficients of v_{dc} to the abovementioned descriptions (based on the expressions provided in equations (1) and (2), arm currents consist of dc, fundamental, and second harmonic components). Therefore, equations (4) and (5) can be rewritten as follows:

$$n_{ux}v_{dc} = \frac{v_{dc}}{2} - \frac{m_{1x}\cos(\omega t - \theta_{m1})}{2}v_{dc} - \frac{m_{2x}\cos(2\omega t - \theta_{m2})}{2}v_{dc} \quad (6)$$

$$n_{lx}v_{dc} = \frac{v_{dc}}{2} + \frac{m_{1x}\cos(\omega t - \theta_{m1})}{2}v_{dc} - \frac{m_{2x}\cos(2\omega t - \theta_{m2})}{2}v_{dc} \quad (7)$$

Therefore, modulation indices (n_{ux} , n_{lx}) are considered having dc, fundamental, and second harmonic components. Accordingly, modulation indices can be expressed as:

$$n_{ux} = \frac{1 - m_{1x}\cos(\omega t - \theta_{m1}) - m_{2x}\cos(2\omega t - \theta_{m2})}{2} \quad (8)$$

$$n_{lx} = \frac{1 + m_{1x}\cos(\omega t - \theta_{m1}) - m_{2x}\cos(2\omega t - \theta_{m2})}{2} \quad (9)$$

Note that modulation indices n_{ux} and n_{lx} are calculated according to the ratio between the sum capacitor voltage and the desired voltage of each arm and thus vary from 0 to 1.

Applying abc to dq0 transform, (8) and (9) can be calculated as:

$$n_u = \left(\frac{1}{2}\right) + \left(\frac{-m_d}{2}\right)\cos(\omega t) + \left(\frac{-m_q}{2}\right)\sin(\omega t) + \left(\frac{-m_{d2}}{2}\right)\cos(2\omega t) + \left(\frac{-m_{q2}}{2}\right)\sin(2\omega t) \quad (10)$$

$$n_l = \left(\frac{1}{2}\right) + \left(\frac{m_d}{2}\right)\cos(\omega t) + \left(\frac{m_q}{2}\right)\sin(\omega t) + \left(\frac{-m_{d2}}{2}\right)\cos(2\omega t) + \left(\frac{-m_{q2}}{2}\right)\sin(2\omega t) \quad (11)$$

where subscripts *d* and *q* represent the two fundamental frequency rotating components at $\omega=2\pi f$, while subscripts *d2,q2* represent the second harmonic rotating components at 2ω, and subscript *0* represents zero sequence component [31].

On the other hand, due to the presence of different harmonic components in both upper and lower arm currents, SM capacitor voltages will sure be affected. This way the sum capacitor voltages include dc, fundamental, and second harmonic components as well. Therefore:

$$U_{cu}^{\Sigma}(t) = U_{cum0}^{\Sigma} + U_{cum1}^{\Sigma}\cos(\omega t - \theta_u) + U_{cum2}^{\Sigma}\cos(2\omega t - \theta_{u2}) \equiv U_{cu0}^{\Sigma} + U_{cud}^{\Sigma} + U_{cuq}^{\Sigma} + U_{cud2}^{\Sigma} + U_{cuq2}^{\Sigma} \quad (12)$$

$$U_{cl}^{\Sigma}(t) = U_{clm0}^{\Sigma} + U_{clm1}^{\Sigma}\cos(\omega t - \theta_l) + U_{clm2}^{\Sigma}\cos(2\omega t - \theta_{l2}) \equiv U_{cl0}^{\Sigma} + U_{cld}^{\Sigma} + U_{clq}^{\Sigma} + U_{cld2}^{\Sigma} + U_{clq2}^{\Sigma} \quad (13)$$

As the aim is to present a standard MMC average model, studying dynamic equations of the converter becomes useful. The stored energy in SM capacitors of each arm can be expressed as follows:

$$W_{cu,l}^{\Sigma} = \frac{1}{2}C\sum_{c=1}^{N}\left(u_{cu,l}\right)^2 \quad (14)$$

Where, u_c represents each SM capacitor voltage. Besides, the embedded capacitor in each SM is considered large enough so that the voltage deviations from the mean value $\frac{U_{cu,l}^{\Sigma}}{N}$ can be neglected. Therefore (14) can be rewritten as:

$$W_{cu,l}^{\Sigma}=\frac{1}{2}\frac{C}{N}\left(U_{cu,l}^{\Sigma}\right)^{2} \tag{15}$$

On the other hand, the instantaneous power injected to each arm equals the energy derivative at any time instant. Therefore:

$$\frac{dW_{cu,l}^{\Sigma}}{dt}=\frac{C}{N}\left(U_{cu,l}^{\Sigma}\right)\left(\frac{dU_{cu,l}^{\Sigma}}{dt}\right)=\left(U_{cu,l}\right)\left(i_{u,l}\right) \tag{16}$$

Substituting $U_{cu,l}=n_{u,l}U_{cu,l}^{\Sigma}$ following dynamics of the sum capacitor voltages are obtained as:

$$\begin{cases}\frac{C}{N}\frac{dU_{cux}^{\Sigma}}{dt}=n_{ux}\,i_{ux}\\ \frac{C}{N}\frac{dU_{clx}^{\Sigma}}{dt}=n_{lx}\,i_{lx}\end{cases} \tag{17}$$

Considering harmonic components of sum capacitor voltage, modulation index, and arm current, the abovementioned equation can be rewritten in dq0 frame as follows:

$$\begin{aligned}&\frac{C}{N}\frac{d}{dt}\left(U_{cu0}^{\Sigma}+U_{cud}^{\Sigma}\cos\omega t+U_{cuq}^{\Sigma}\sin\omega t+U_{cud2}^{\Sigma}\cos 2\omega t+U_{cuq2}^{\Sigma}\sin 2\omega t\right)=\\&\left(\frac{1}{2}+\frac{-m_d}{2}\cos\omega t+\frac{-m_q}{2}\sin\omega t+\frac{-m_{d2}}{2}\cos 2\omega t+\frac{-m_{q2}}{2}\sin 2\omega t\right)\left(i_{uo}+i_{ud}\cos\omega t+i_{uq}\sin\omega t+i_{ud2}\cos 2\omega t+i_{uq2}\sin 2\omega t\right)\end{aligned} \tag{18}$$

which leads to:

$$\begin{aligned}&\frac{C}{N}\left(\frac{d}{dt}U_{cu0}^{\Sigma}+\frac{d}{dt}U_{cud}^{\Sigma}\cos\omega t-\omega U_{cud}^{\Sigma}\sin\omega t+\frac{d}{dt}U_{cuq}^{\Sigma}\sin\omega t+\omega U_{cuq}^{\Sigma}\cos\omega t+\frac{d}{dt}U_{cud2}^{\Sigma}\cos 2\omega t-2\omega U_{cud2}^{\Sigma}\sin 2\omega t\right.\\&\left.\quad+\frac{d}{dt}U_{cuq2}^{\Sigma}\sin 2\omega t+2\omega U_{cuq2}^{\Sigma}\cos 2\omega t\right)=\\&\left(\frac{1}{2}+\frac{-m_d}{2}\cos\omega t+\frac{-m_q}{2}\sin\omega t+\frac{-m_{d2}}{2}\cos 2\omega t+\frac{-m_{q2}}{2}\sin 2\omega t\right)\left(i_{uo}+i_{ud}\cos\omega t+i_{uq}\sin\omega t+i_{ud2}\cos 2\omega t+i_{uq2}\sin 2\omega t\right)\end{aligned} \tag{19}$$

Multiplying the two expressions in right hand side of the equation (19), different harmonic components of the product signal can be represented in different matrix rows. Meanwhile, the multiplication and harmonic separation process is clearly expressed in the appendix. Therefore:

$$\begin{aligned}\frac{C}{N}\frac{d}{dt}\begin{bmatrix}U_{cud}^{\Sigma}\\U_{cuq}^{\Sigma}\\U_{cud2}^{\Sigma}\\U_{cuq2}^{\Sigma}\\U_{cu0}^{\Sigma}\end{bmatrix}&=\frac{C}{N}\begin{bmatrix}0&\omega&0&0&0\\-\omega&0&0&0&0\\0&0&0&2\omega&0\\0&0&-2\omega&0&0\\0&0&0&0&0\end{bmatrix}\begin{bmatrix}U_{cud}^{\Sigma}\\U_{cuq}^{\Sigma}\\U_{cud2}^{\Sigma}\\U_{cuq2}^{\Sigma}\\U_{cu0}^{\Sigma}\end{bmatrix}+\\&\begin{bmatrix}-\frac{m_d}{2}i_{uo}+\frac{1}{2}i_{ud}-\frac{m_{d2}}{4}i_{ud}-\frac{m_{q2}}{4}i_{uq}-\frac{m_d}{4}i_{ud2}-\frac{m_q}{4}i_{uq2}\\-\frac{m_q}{2}i_{uo}+\frac{1}{2}i_{uq}+\frac{m_{d2}}{4}i_{uq}-\frac{m_{q2}}{4}i_{ud}+\frac{m_q}{4}i_{ud2}-\frac{m_d}{4}i_{uq2}\\-\frac{m_d}{4}i_{ud}+\frac{m_q}{4}i_{uq}-\frac{m_{d2}}{2}i_{u0}+\frac{1}{2}i_{ud2}\\-\frac{m_q}{4}i_{ud}-\frac{m_d}{4}i_{uq}-\frac{m_{q2}}{2}i_{u0}+\frac{1}{2}i_{uq2}\\\frac{1}{2}i_{u0}-\frac{m_d}{4}i_{ud}-\frac{m_q}{4}i_{uq}-\frac{m_{d2}}{4}i_{ud2}-\frac{m_{q2}}{4}i_{uq2}\end{bmatrix}\end{aligned} \tag{20}$$

On the other hand, applying KVL to Fig. 1(a) leads to:

$$L_c \frac{di_x}{dt} + R_c i_x + v_{gx} = \frac{v_{dc}}{2} - n_{ux} U_{cux}^{\Sigma} - L_{arm} \frac{di_{ux}}{dt} - R_{arm} i_{ux} \tag{21}$$

Since $i_x = i_{ux} - i_{lx}$, previous equation can be rewritten as:

$$(L_c + L_{arm}) \frac{di_{ux}}{dt} - L_c \frac{di_{lx}}{dt} = -(R_c + R_{arm}) i_{ux} + R_c i_{lx} - v_{gx} + \frac{v_{dc}}{2} - n_{ux} U_{cux}^{\Sigma} \tag{22}$$

Finally, according to (10)-(13) and appendix notes, the MMC dynamic state-space equation could be derived in dq frame as:

$$\begin{aligned}
&(L_c + L_{arm}) \frac{d}{dt} \begin{bmatrix} i_{ud} \\ i_{uq} \\ i_{uo} \end{bmatrix} - L_c \frac{d}{dt} \begin{bmatrix} i_{ld} \\ i_{lq} \\ i_{lo} \end{bmatrix} = \begin{bmatrix} -(R_c + R_{arm}) & (L_c + L_{arm})\omega & 0 \\ -(L_c + L_{arm})\omega & -(R_c + R_{arm}) & 0 \\ 0 & 0 & -(R_c + R_{arm}) \end{bmatrix} \begin{bmatrix} i_{ud} \\ i_{uq} \\ i_{uo} \end{bmatrix} + \begin{bmatrix} R_c & -L_c\omega & 0 \\ L_c\omega & R_c & 0 \\ 0 & 0 & R_c \end{bmatrix} \begin{bmatrix} i_{ld} \\ i_{lq} \\ i_{lo} \end{bmatrix} - \begin{bmatrix} v_{gd} \\ v_{gq} \\ 0 \end{bmatrix} + \begin{bmatrix} 0 \\ 0 \\ \frac{v_{dc}}{2} \end{bmatrix} \\
&- \begin{bmatrix} -\frac{m_d}{2} U_{cu0}^{\Sigma} + \frac{1}{2} U_{cud}^{\Sigma} - \frac{m_{d2}}{4} U_{cud}^{\Sigma} - \frac{m_{q2}}{4} U_{cuq}^{\Sigma} - \frac{m_d}{4} U_{cud2}^{\Sigma} - \frac{m_q}{4} U_{cuq2}^{\Sigma} \\ -\frac{m_q}{2} U_{cu0}^{\Sigma} + \frac{1}{2} U_{cuq}^{\Sigma} + \frac{m_{d2}}{4} U_{cuq}^{\Sigma} - \frac{m_{q2}}{4} U_{cud}^{\Sigma} + \frac{m_q}{4} U_{cud2}^{\Sigma} - \frac{m_d}{4} U_{cuq2}^{\Sigma} \\ \frac{1}{2} U_{cu0}^{\Sigma} - \frac{m_d}{4} U_{cud}^{\Sigma} - \frac{m_q}{4} U_{cuq}^{\Sigma} - \frac{m_{d2}}{4} U_{cud2}^{\Sigma} - \frac{m_{q2}}{4} U_{cuq2}^{\Sigma} \end{bmatrix}
\end{aligned} \tag{23}$$

3. Steady-State Operation Analysis of the Proposed Model

In order to calculate modulation indices in steady-state operation mode of the converter, all quantities should be replaced with their reference values in stable mode. In this regard, all derivative values in (20) are equated to zero as well as second harmonic components of currents. Also, m_{d2} and m_{q2} could be neglected based on designed controllers.

Zero component of sum capacitor voltages (U_{cu0}^{Σ}) is equal to dc-link voltage reference (V_r). Accordingly, from the last row of matrix (20), (24) can be expressed as:

$$i_{u0} = \frac{m_{ds}}{2} i_{ud} + \frac{m_{qs}}{2} i_{uq} \tag{24}$$

In the same way, other quantities can be calculated as:

$$U_{cud}^{\Sigma} = \frac{-N\left(m_{qs}^2 - 2\right)}{4C\omega} i_{uq} \tag{25}$$

$$U_{cuq}^{\Sigma} = \frac{N\left(m_{ds}^2 - 2\right)}{4C\omega} i_{ud} \tag{26}$$

$$U_{cud2}^{\Sigma} = -\frac{Nm_{qs}}{8C\omega} i_{ud} - \frac{Nm_{ds}}{8C\omega} i_{uq} \tag{27}$$

$$U_{cuq2}^{\Sigma} = \frac{Nm_{ds}}{8C\omega} i_{ud} - \frac{Nm_{qs}}{8C\omega} i_{uq} \tag{28}$$

On the other hand, the instantaneous variations in reference values of arm currents should be considered in control algorithm to obtain the best performance during changes from transient to steady-state operating modes of the interfaced converter. Consequently:

$$\frac{di_{ud}}{dt}=I^{*}_{avud}=\frac{I^{*}_{avd}}{2}\ ,\ \frac{di_{uq}}{dt}=I^{*}_{avuq}=\frac{I^{*}_{avq}}{2},\ \frac{di_{ld}}{dt}=I^{*}_{avld}=-\frac{I^{*}_{avd}}{2}\ ,\ \frac{di_{lq}}{dt}=I^{*}_{avlq}=-\frac{I^{*}_{avq}}{2} \tag{29}$$

Substituting instantaneous currents with their reference values gives:

$$i_{ud}=I^{*}_{ud}=\frac{I^{*}_{d}}{2}\ ,\ i_{uq}=I^{*}_{uq}=\frac{I^{*}_{q}}{2}\ ,\ i_{ld}=I^{*}_{ld}=-\frac{I^{*}_{d}}{2}\ ,\ i_{lq}=I^{*}_{lq}=-\frac{I^{*}_{q}}{2},\ i_{u0}=i_{l0}=I^{*}_{0} \tag{30}$$

Therefore, by substituting (24)-(30) in (23), steady-state equations of the proposed model can be expressed as:

$$\begin{bmatrix} L_c+\frac{L_{arm}}{2} & 0 & 0 \\ 0 & L_c+\frac{L_{arm}}{2} & 0 \\ \frac{m_{ds}}{4}L_{arm} & \frac{m_{qs}}{4}L_{arm} & 0 \end{bmatrix}\begin{bmatrix} I^{*}_{avd} \\ I^{*}_{avq} \\ V_r \end{bmatrix}=-\begin{bmatrix} V^{*}_{gd} \\ V^{*}_{gq} \\ 0 \end{bmatrix}+\begin{bmatrix} -\left(R_c+\frac{R_{arm}}{2}\right) & \left(L_c+\frac{L_{arm}}{2}\right)\omega+\frac{N\left(3m_{qs}^2-m_{ds}^2-8\right)}{64C\omega} & \frac{m_{ds}}{2} \\ -\left(L_c+\frac{L_{arm}}{2}\right)\omega-\frac{N\left(3m_{ds}^2-m_{qs}^2-8\right)}{64C\omega} & -\left(R_c+\frac{R_{arm}}{2}\right) & \frac{m_{qs}}{2} \\ -\frac{8m_{ds}C\omega R_{arm}+2Nm_{qs}}{32C\omega} & -\frac{8m_{qs}C\omega R_{arm}-2Nm_{ds}}{32C\omega} & 0 \end{bmatrix}\begin{bmatrix} I^{*}_{d} \\ I^{*}_{q} \\ V_r \end{bmatrix} \tag{31}$$

Last row of (31) leads to:

$$m_{ds}\underbrace{\left(\frac{L_{arm}}{4}I^{*}_{avd}+\frac{R_{arm}}{4}I^{*}_{d}-\frac{N}{16C\omega}I^{*}_{q}\right)}_{A}=m_{qs}\underbrace{\left(-\frac{L_{arm}}{4}I^{*}_{avq}-\frac{R_{arm}}{4}I^{*}_{q}-\frac{N}{16C\omega}I^{*}_{d}\right)}_{B} \tag{32}$$

It is obvious that A and B are constant values, so there would be a linear relation between m_{ds} and m_{qs}. Thus, first row of (31) can lead to a quadratic equation in terms of m_{ds} as:

$$\frac{\left(3NA^2-B^2\right)I^{*}_{q}}{64C\omega B^2}m_{ds}^2+\frac{V_r}{2}m_{ds}=V^{*}_{gd}+\left(L_c+\frac{L_{arm}}{2}\right)I^{*}_{avd}+\left(R_c+\frac{R_{arm}}{2}\right)I^{*}_{d}-\left(L_c+\frac{L_{arm}}{2}\right)\omega I^{*}_{q}+\frac{1}{8C\omega}I^{*}_{q} \tag{33}$$

By solving the quadratic equation above, m_{ds} and m'_{ds} can be calculated as:

$$\begin{cases} m_{ds}=\dfrac{-16C\omega B^2V_r}{\left(3NA^2-B^2\right)I^{*}_{q}}+\dfrac{\sqrt{\frac{V_r^2}{4}-\left(\frac{\left(3NA^2-B^2\right)I^{*}_{q}}{16C\omega B^2}\right)\left(V^{*}_{gd}+\left(L_c+\frac{L_{arm}}{2}\right)I^{*}_{avd}+\left(R_c+\frac{R_{arm}}{2}\right)I^{*}_{d}-\left(L_c+\frac{L_{arm}}{2}\right)\omega I^{*}_{q}+\frac{1}{8C\omega}I^{*}_{q}\right)}}{\frac{\left(3NA^2-B^2\right)I^{*}_{q}}{32C\omega B^2}} \\ m'_{ds}=\dfrac{-16C\omega B^2V_r}{\left(3NA^2-B^2\right)I^{*}_{q}}-\dfrac{\sqrt{\frac{V_r^2}{4}-\left(\frac{\left(3NA^2-B^2\right)I^{*}_{q}}{16C\omega B^2}\right)\left(V^{*}_{gd}+\left(L_c+\frac{L_{arm}}{2}\right)I^{*}_{avd}+\left(R_c+\frac{R_{arm}}{2}\right)I^{*}_{d}-\left(L_c+\frac{L_{arm}}{2}\right)\omega I^{*}_{q}+\frac{1}{8C\omega}I^{*}_{q}\right)}}{\frac{\left(3NA^2-B^2\right)I^{*}_{q}}{32C\omega B^2}} \end{cases} \tag{34}$$

Then, substituting them in (32), m_{qs} and m'_{qs} can be calculated.

Besides that, controlling some other features such as circulating current and capacitor voltage are of importance in MMC operation.

A. Circulating current control

The circulating currents, caused by the internal voltage differences between each phase and the dc-link, consist of a dc and a second harmonic component. The dc term is in charge of dc to ac power transfer while the ac term does not affect the ac-side output voltages and currents.

However, it increases the *rms* values of currents in each arm resulting in higher power losses and thus, should be eliminated. Assuming $\theta = 2\omega t$, the phase sequence used in the transformation to the rotational reference frame is *a-c-b*. Applying the transformation, the KVL in converter phase loops becomes as follows:

$$L_{arm}\frac{d}{dt}\begin{bmatrix} i_{ud\,2} \\ i_{uq\,2} \end{bmatrix} = \begin{bmatrix} -R_{arm} & 2L_{arm}\,\omega \\ -2L_{arm}\,\omega & -R_{arm} \end{bmatrix}\begin{bmatrix} i_{ud\,2} \\ i_{uq\,2} \end{bmatrix} - \begin{bmatrix} -\frac{m_d}{4}U^{\Sigma}_{cud} + \frac{m_q}{4}U^{\Sigma}_{cuq} - \frac{m_{d\,2}}{2}U^{\Sigma}_{cu\,0} + \frac{1}{2}U^{\Sigma}_{cud\,2} \\ -\frac{m_q}{4}U^{\Sigma}_{cud} - \frac{m_d}{4}U^{\Sigma}_{cuq} - \frac{m_{q\,2}}{2}U^{\Sigma}_{cu\,0} + \frac{1}{2}U^{\Sigma}_{cuq\,2} \end{bmatrix} \tag{35}$$

In order to achieve a stable operation of MMC, second harmonic currents are desired to be zero. In such case, second harmonic components of modulation indices can be evaluated and then disposed to zero.

$$m_{d\,2s} = \frac{2}{U^{\Sigma}_{cu\,0}}\left[L_{arm}\frac{d}{dt}i_{ud\,2} + R_{arm}\,i_{ud\,2} - 2L_{arm}\,\omega i_{uq\,2} - \frac{m_{ds}}{4}U^{\Sigma}_{cud} + \frac{m_{qs}}{4}U^{\Sigma}_{cuq} + \frac{1}{2}U^{\Sigma}_{cud\,2}\right] \tag{36}$$

$$m_{q\,2s} = \frac{2}{U^{\Sigma}_{cu\,0}}\left[L_{arm}\frac{d}{dt}i_{uq\,2} + R_{arm}\,i_{uq\,2} + 2L_{arm}\,\omega i_{ud\,2} - \frac{m_{qs}}{4}U^{\Sigma}_{cud} - \frac{m_{ds}}{4}U^{\Sigma}_{cuq} + \frac{1}{2}U^{\Sigma}_{cuq\,2}\right] \tag{37}$$

B. Capacitor voltage balancing algorithm

The most popular capacitor voltage-balancing method applied to MMCs, is based on a sorting algorithm, in which, the voltages of SM capacitors in each arm are measured and sorted during every control period. Then, based on the direction of arm current, the required number of SMs having the lowest (or highest) voltage values will be switched on. The only weakness is that the accomplishment of the sorting algorithm during every control period leads to unnecessary switching transitions within SMs. Since the algorithm is applied to all sorted SMs, regardless of their previous states, switching may occur even at a constant number of inserted SMs.

To improve this high switching frequency, a new voltage-balancing method based on a reduced switching frequency (RSF) has been modified [32]. In this method, ΔN (which is the number of SMs that should be added in the next control period) is expressed as $N_{new} - N_{old}$ (where N_{old} is the current number of switches in on state and N_{new} is the newly expected number), as shown in Fig. 2.

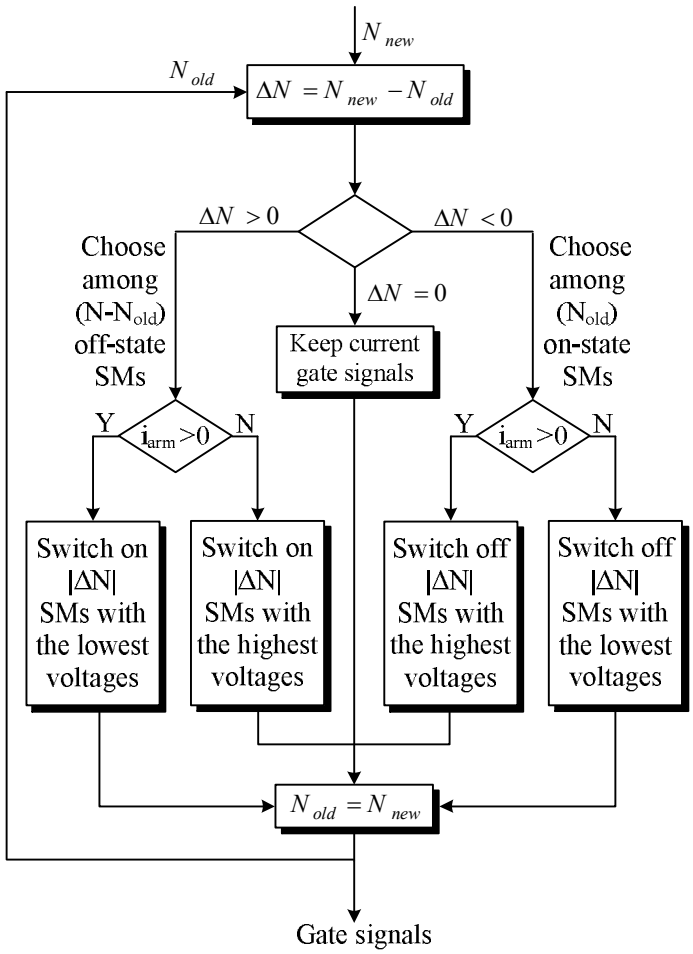

Fig. 2.RSF capacitor voltage balancing algorithm applied to each arm.

According to the direction of arm currents $\left(i_{arm} : i_{ux} \;\; or \;\; i_{lx}\right)$, switching transitions of each arm will be performed as follows:

- If ΔN is positive and additional SMs are needed to be switched on, the selection process will only take place between SMs in the off-state. This way, charging current $\left(i_{arm} > 0\right)$ leads to the selection of SMs with lowest voltage values while $\left(i_{arm} < 0\right)$ turns on SMs with highest capacitor voltages.
- If ΔN is negative and the number of the on-state SMs needs to be reduced, the selection process will only take place between SMs in the on-state and no more SMs will be switched on. Therefore, charging current $\left(i_{arm} > 0\right)$ leads to the selection of SMs with highest voltage values while $\left(i_{arm} < 0\right)$ turns off SMs with lowest capacitor voltages.

It should be noted that in comparison with the conventional algorithms, RSF voltage balancing method can considerably reduce the overall switching losses by lowering the average switching frequency. The general schematic diagram and principle of the proposed control method is shown in Fig. 3.

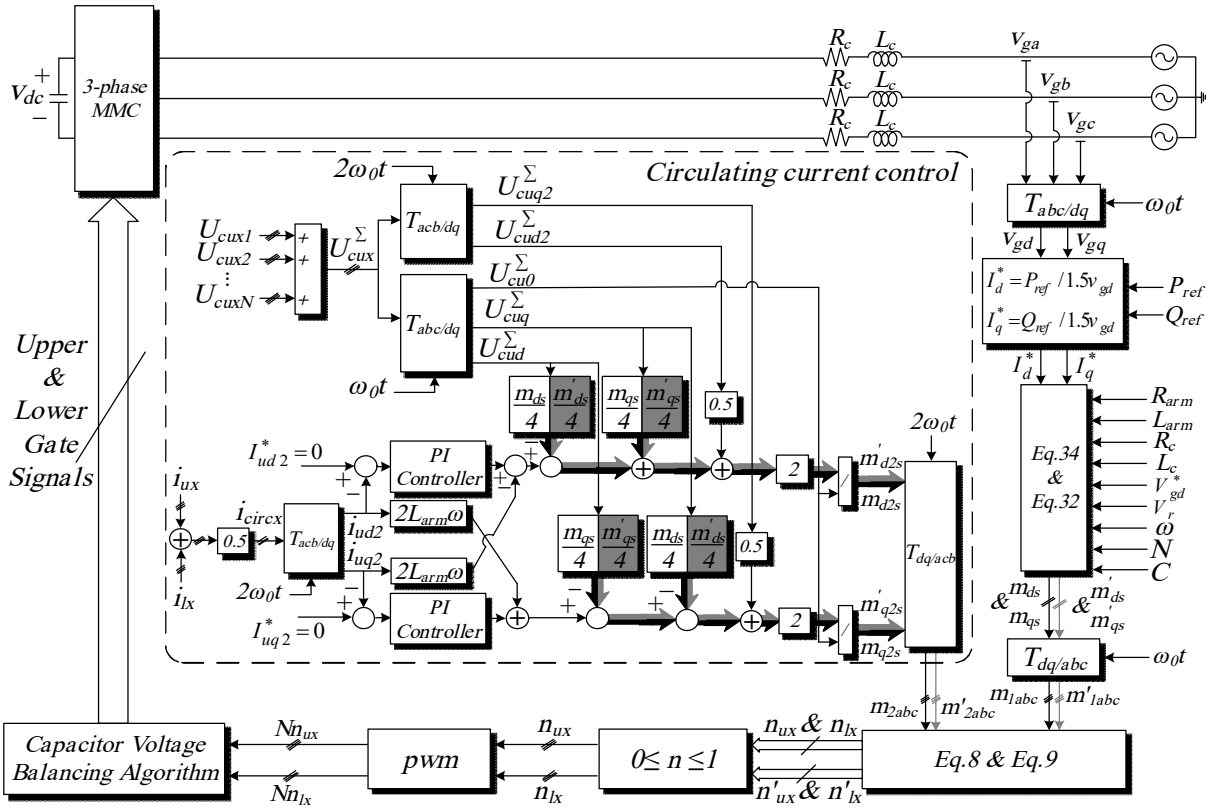

Fig. 3. General schematic diagram of the proposed control method for control of MMCs in grid-connected mode.

C. Maximum stable operation range

The converter can deliver a certain amount of power which depends on different structural components and therefore, the margin should be eliminated in order to guarantee the stability of operation. Neglecting losses, power transfer from dc to ac can be expressed as:

$$v_{dc}i_{dc} = -\left(v_d i_d + v_q i_q\right) \tag{38}$$

Applying KVL to the output of MMC shown in Fig. 1(a) results in equations describing converter voltages which then, can be transferred to dq frame as:

$$v_d = v_{gd} + R_c i_d + L_c \frac{di_d}{dt} - \omega L_c i_q \tag{39}$$

$$v_q = v_{gq} + R_c i_q + L_c \frac{di_q}{dt} + \omega L_c i_d \tag{40}$$

Therefore, replacing (39) and (40) in (38) leads to:

$$v_{dc}i_{dc} = -\left(v_{gd} i_d + R_c i_d^2 + L_c i_d \frac{di_d}{dt} - \omega L_c i_q i_d + v_{gq} i_q + R_c i_q^2 + L_c i_q \frac{di_q}{dt} + \omega L_c i_d i_q\right) \tag{41}$$

Replacing time derivatives of currents with average values and then dividing both sides of (41) by R_c leads to:

$$i_d^2 + \frac{L_c}{R_c} i_d i_{avd} + \frac{v_{gd}}{R_c} i_d + i_q^2 + \frac{L_c}{R_c} i_q i_{avq} + \frac{v_{gq}}{R_c} i_q = -\frac{v_{dc}i_{dc}}{R_c} \tag{42}$$

Then the terms $\left(\frac{L_c i_{avd} + v_{gd}}{2R_c}\right)^2$ and $\left(\frac{L_c i_{avq} + v_{gq}}{2R_c}\right)^2$ are added to the both sides of the equation.

Therefore:

$$\left[i_d^2 + \left(\frac{L_c i_{avd} + v_{gd}}{R_c}\right) i_d + \left(\frac{L_c i_{avd} + v_{gd}}{2R_c}\right)^2\right] + \left[i_q^2 + \left(\frac{L_c i_{avq} + v_{gq}}{R_c}\right) i_q + \left(\frac{L_c i_{avq} + v_{gq}}{2R_c}\right)^2\right] = -\frac{v_{dc} i_{dc}}{R_c} + \left(\frac{L_c i_{avd} + v_{gd}}{2R_c}\right)^2 + \left(\frac{L_c i_{avq} + v_{gq}}{2R_c}\right)^2 \quad (43)$$

Finally, converter's current curve can be obtained as (44):

$$\left(i_d + \frac{L_c i_{avd} + v_{gd}}{2R_c}\right)^2 + \left(i_q + \frac{L_c i_{avq} + v_{gq}}{2R_c}\right)^2 = \left(\left(L_c i_{avd} + v_{gd}\right)^2 + \left(L_c i_{avq} + v_{gq}\right)^2 - 4R_c v_{dc} i_{dc}\right) / \left(4R_c^2\right) \quad (44)$$

Considering $P = \frac{3}{2} v_{gd} i_d$ and $Q = \frac{3}{2} v_{qd} i_q$, active and reactive power curve of MMC can be obtained as:

$$\left(P + \frac{3v_{gd} L_c i_{avd} + 3v_{gd}^2}{4R_c}\right)^2 + \left(Q + \frac{3v_{gd} L_c i_{avq}}{4R_c}\right)^2 = \left(\left(3v_{gd} L_c i_{avd} + 3v_{gd}^2\right)^2 + \left(3v_{gd} L_c i_{avq}\right)^2 - 36v_{gd}^2 R_c v_{dc} i_{dc}\right) / \left(8R_c^2\right) \quad (45)$$

On the other hand, considering first row of (35) as in steady-state operation mode, following equation can be achieved.

$$\frac{m_d}{4} U_{cud}^{\Sigma} - \frac{m_q}{4} U_{cuq}^{\Sigma} - \frac{1}{2} U_{cud\,2}^{\Sigma} = 0 \quad (46)$$

Then, using (25)-(28), it can be rewritten as follows:

$$\frac{-Nm_{ds}\left(m_{qs}^2 - 2\right)}{16C\omega} \frac{I_q^*}{2} - \frac{Nm_{qs}\left(m_{ds}^2 - 2\right)}{16C\omega} \frac{I_d^*}{2} + \frac{Nm_{qs}}{16C\omega} \frac{I_d^*}{2} + \frac{Nm_{ds}}{16C\omega} \frac{I_q^*}{2} = 0 \quad (47)$$

Applying simplifications to the above equation leads to:

$$\frac{Nm_{ds}}{16C\omega} I_q^* + \frac{Nm_{qs}}{16C\omega} I_d^* + \frac{Nm_{qs}}{16C\omega} \frac{I_d^*}{2} + \frac{Nm_{ds}}{16C\omega} \frac{I_q^*}{2} = 0 \quad (48)$$

Therefore,

$$3Nm_{ds} I_q^* + 3Nm_{qs} I_d^* = 0\,. \quad (49)$$

This way (50) can be derived as:

$$\frac{m_{ds}}{m_{qs}} = -\frac{I_d^*}{I_q^*} \quad (50)$$

Replacing (32) in (50) gives:

$$\frac{I_d^*}{I_q^*} = \frac{\frac{L_{arm}}{4} I_{avq}^* + \frac{R_{arm}}{4} I_q^* + \frac{N}{16C\omega} I_d^*}{\frac{L_{arm}}{4} I_{avd}^* + \frac{R_{arm}}{4} I_d^* - \frac{N}{16C\omega} I_q^*} \quad (51)$$

Multiplying two sides of (51) leads to:

$$\frac{L_{arm}}{4}I_d^*I_{avd}^* + \frac{R_{arm}}{4}\left(I_d^*\right)^2 - \frac{N}{16C\omega}I_d^*I_q^* = \frac{L_{arm}}{4}I_q^*I_{avq}^* + \frac{R_{arm}}{4}\left(I_q^*\right)^2 + \frac{N}{16C\omega}I_q^*I_d^* \tag{52}$$

Applying simplifications to the above equation leads to:

$$I_d^{*2} + \frac{L_{arm}}{R_{arm}}I_d^*I_{avd}^* - I_q^{*2} - \frac{L_{arm}}{R_{arm}}I_q^*I_{avq}^* = 0 \tag{53}$$

Then the two components of $\left(\frac{L_{arm}}{2R_{arm}}I_{avd}^*\right)^2$ and $-\left(\frac{L_{arm}}{2R_{arm}}I_{avq}^*\right)^2$ are added to both sides of the above equation as:

$$\left(I_d^{*2} + \frac{L_{arm}}{R_{arm}}I_d^*I_{avd}^* + \left(\frac{L_{arm}}{2R_{arm}}I_{avd}^*\right)^2\right) - \left(I_q^{*2} + \frac{L_{arm}}{R_{arm}}I_q^*I_{avq}^* + \left(\frac{L_{arm}}{2R_{arm}}I_{avq}^*\right)^2\right) = \left(\frac{L_{arm}}{2R_{arm}}I_{avd}^*\right)^2 - \left(\frac{L_{arm}}{2R_{arm}}I_{avq}^*\right)^2 \tag{54}$$

This can be rewritten in the form of:

$$\left(I_q^* + \frac{L_{arm}}{2R_{arm}}I_{avq}^*\right)^2 - \left(I_d^* + \frac{L_{arm}}{2R_{arm}}I_{avd}^*\right)^2 = \frac{L_{arm}^2}{4R_{arm}^2}\left(I_{avq}^{*2} - I_{avd}^{*2}\right) \tag{55}$$

Considering $P = \frac{3}{2}v_{gd}i_d$ and $Q = \frac{3}{2}v_{qd}i_q$, (56) can be obtained as:

$$\left(Q_{ref} + \frac{3L_{arm}}{4R_{arm}}v_{gd}I_{avq}^*\right)^2 - \left(P_{ref} + \frac{3L_{arm}}{4R_{arm}}v_{gd}I_{avd}^*\right)^2 = \frac{9L_{arm}^2}{16R_{arm}^2}v_{gd}^2\left(I_{avq}^{*2} - I_{avd}^{*2}\right) \tag{56}$$

Equation (44) describes a circle with the center of $\left(-\frac{L_ci_{avd}+v_{gd}}{2R_c}, -\frac{L_ci_{avq}+v_{gq}}{2R_c}\right)$ and radius of $\sqrt{\left(\left(L_ci_{avd}+v_{gd}\right)^2 + \left(L_ci_{avq}+v_{gq}\right)^2 - 4R_cv_{dc}i_{dc}\right)/\left(4R_c^2\right)}$, while (55) is the equation for a hyperbolic. By drawing them together, we can estimate the current curve for the stable operation of MMC in the proposed model (Fig. 4(a)). The power flow curve of MMC shown in Fig. 4(b) can also be derived in the same way.

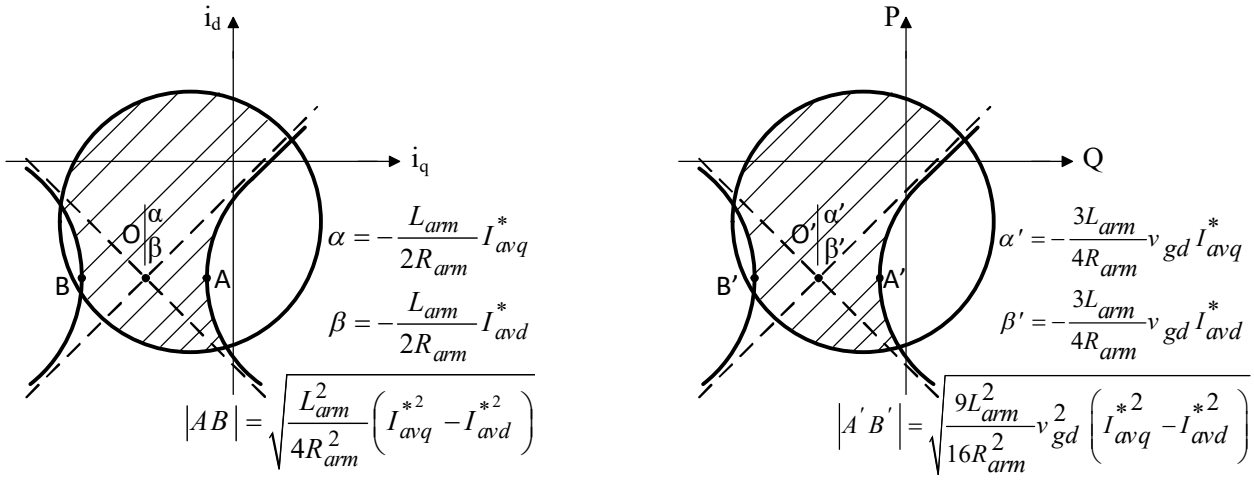

Fig. 4.Region for stable operation of MMCs in grid-connected operating mode, (a) current curve, (b) P-Q curve.

4. Results and Discussion

The detailed model is simulated in MATLAB/Simulink in order to verify operation of the proposed control and switching method in control and operation of MMCs in power system. The values of different circuit components and operational conditions applied to simulations are listed in Table I.

Fig. 5(a) shows the modulation index of the upper arm of phase-a (n_{ua}), generated by the proposed modulation method. Implying that, a carrier-based modulation with phase opposition disposition (POD) carriers is used in which individual triangular carriers are applied for each cell. Applying this fixed PWM pattern to switching functions of each phase, the inner emfs of each phase leg driving output currents of MMC are obtained based on total arm voltages as:

$$e_x = \frac{U_{clx} - U_{cux}}{2} \tag{55}$$

As shown in Fig. 5(b), these voltage levels are fixed at desired values which mean that the balancing algorithm is working properly.

In order to verify the efficiency of RSF voltage balancing algorithm, a comparison is also provided. Fig. 6(a) illustrates the gate signal applied to the first SM in the upper arm of phase-a (G_{ua1}) while conventional voltage balancing algorithm is applied. Applying RSF algorithm, G_{ua1} is then again demonstrated in Fig. 6(b). The comparison results clearly show an effective reduction in switching frequency as the RSF algorithm avoids unnecessary switching transitions.

Table 1. MMC Parameters and Operational Conditions Applied to Simulations

Items	Values
ac system voltage V_g^* (L-L,rms)	10 kV
ac system inductance L_c	30 mH
ac system resistance R_c	0.5 Ω
dc bus voltage V_r	20 kV
Number of SMs per arm N	20
SM capacitance C	10000 μF
Arm inductance L_{arm}	9 mH
Arm equivalent resistance R_{arm}	0.7 Ω
SM capacitor voltage V_{csm}	1 kV
Carrier frequency f_{sw}	5 kHz
active power P_{ref}	14 MW
reactive power Q_{ref}	6 Mvar

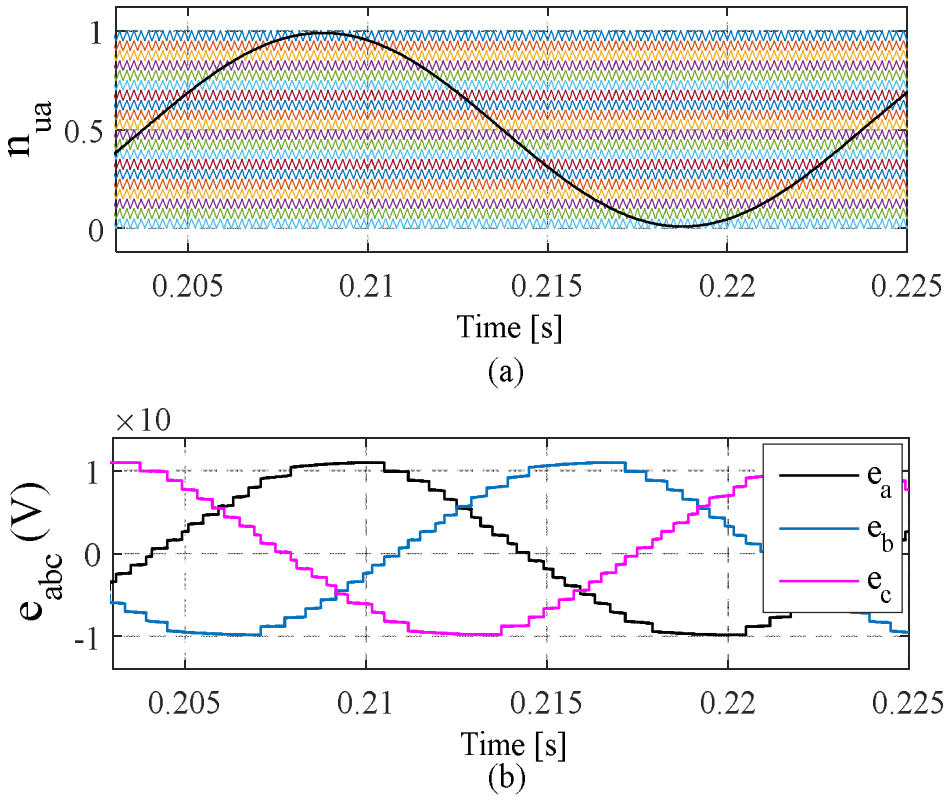

Fig. 5. Applied modulation method, (a) modulation index of the upper arm in phase-a generated by the proposed modulation method, (b) inner emfs of phase legs.

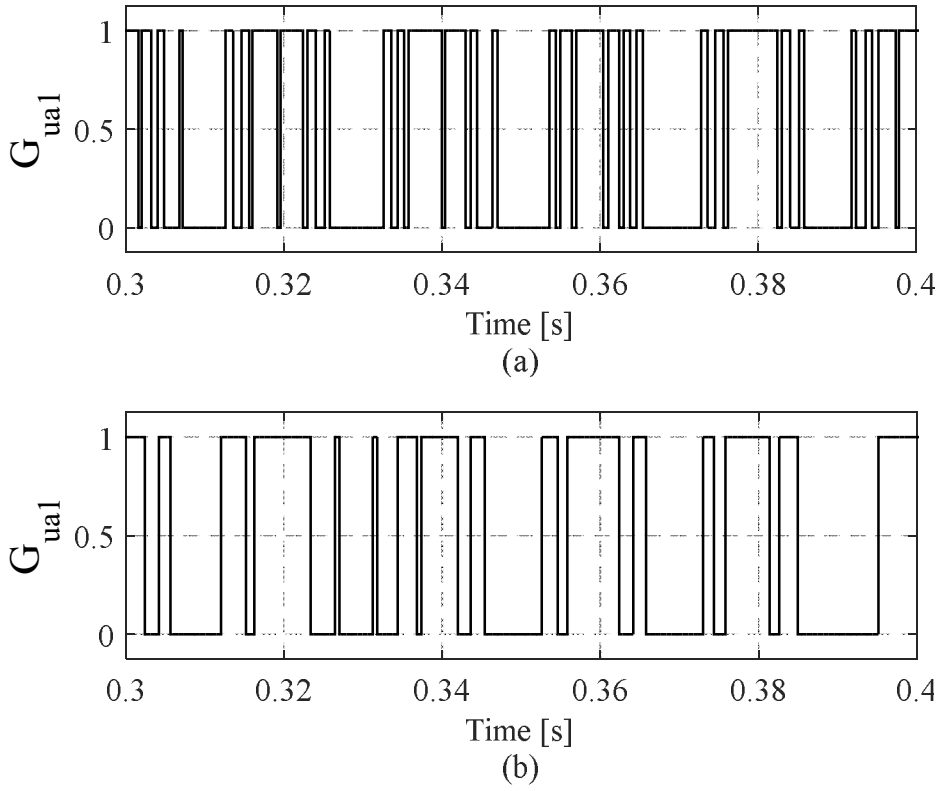

Fig. 6. Gate signals applied to the first SM of upper arm in phase-a, (a) conventional voltage balancing algorithm, (b) RSF voltage balancing algorithm.

In order to validate the proposed circulating current control, as it can be seen in Fig. 7(a), the algorithm is initially disabled but then re-enabled at 0.4 s. As can be seen, the harmonic part of the circulating current is reduced effectively while appropriate components generated by the controller are added to modulation indices. Using this procedure leads to a more sinusoidal arm current waveform as the distortion is mitigated. Fig. 7(b) illustrates the upper arm current of phase-a. It should be noted that the dc component in the arm current is necessary as it represents the transmission of active power between the ac and dc sides. Fig. 7(c) represents SM capacitor voltages of upper arm for phase-a. The voltages are in the reasonable criteria and well balanced as well as the significant reduction of the voltage fluctuation is achieved. It should be noted that similar to any other controlling process, there is a transient period which happens inevitably before complete accomplishment of steady state operation. In this regard, it can be seen that the arm current as well as SM capacitor voltages are dealing with some oscillations during this transient period which by the way ends perfectly at 0.55 s when the desired steady state operation can be achieved as well.

Output voltages and currents of the converter are shown in Fig. 7(d) and Fig. 7(e), respectively. Since circulating currents are considered as interior quantities, adverse effects of the controller on the outer dynamic performances of the converter are not desirable. Consistent with this concept, the ac-side quantities seem to remain the same and without any significant changes. However, a slight reduction in output voltage THD is obtained, which could be considered as a result of the reductions occurred in the SMs' voltage fluctuations. Hence, the controller improves output voltage quality as well as the inner dynamic performances.

In order to validate the proposed controller, all L_{arm}, L_c, and C quantities used in simulations have been changed by an amount of ±%20 and the results are demonstrated. As it can be seen in Fig.8 (a), increasing L_{arm}, L_c, and C values results in lower circulating current amount which then leads to a more sinusoidal arm current and less fluctuations in capacitor voltages (shown in Fig. 8(b) and Fig. 8(c) respectively). Applying the proposed circulating current control at 0.4s, the second harmonic component of current has been eliminated effectively and the overall performance of the converter is improved as it can be seen in the simulation results.

Applying 20% decrease to L_{arm}, L_c, and C values, circulating current has been significantly increased as it is demonstrated in Fig. 9(a). This way the arm current is containing more harmonic components and the capacitor voltage fluctuations are increased as well. As it can be seen in Fig. 9(a), applying the proposed circulating current at 0.4s leads to a significant reduction in second harmonic component of circulating current. Also the more sinusoidal arm current waveform and reduced capacitor voltage fluctuations have been demonstrated in Fig. 9(b) and Fig. 9(c)

respectively. Therefore, the desired MMC operation based on the proposed modulation and control method has been validated.

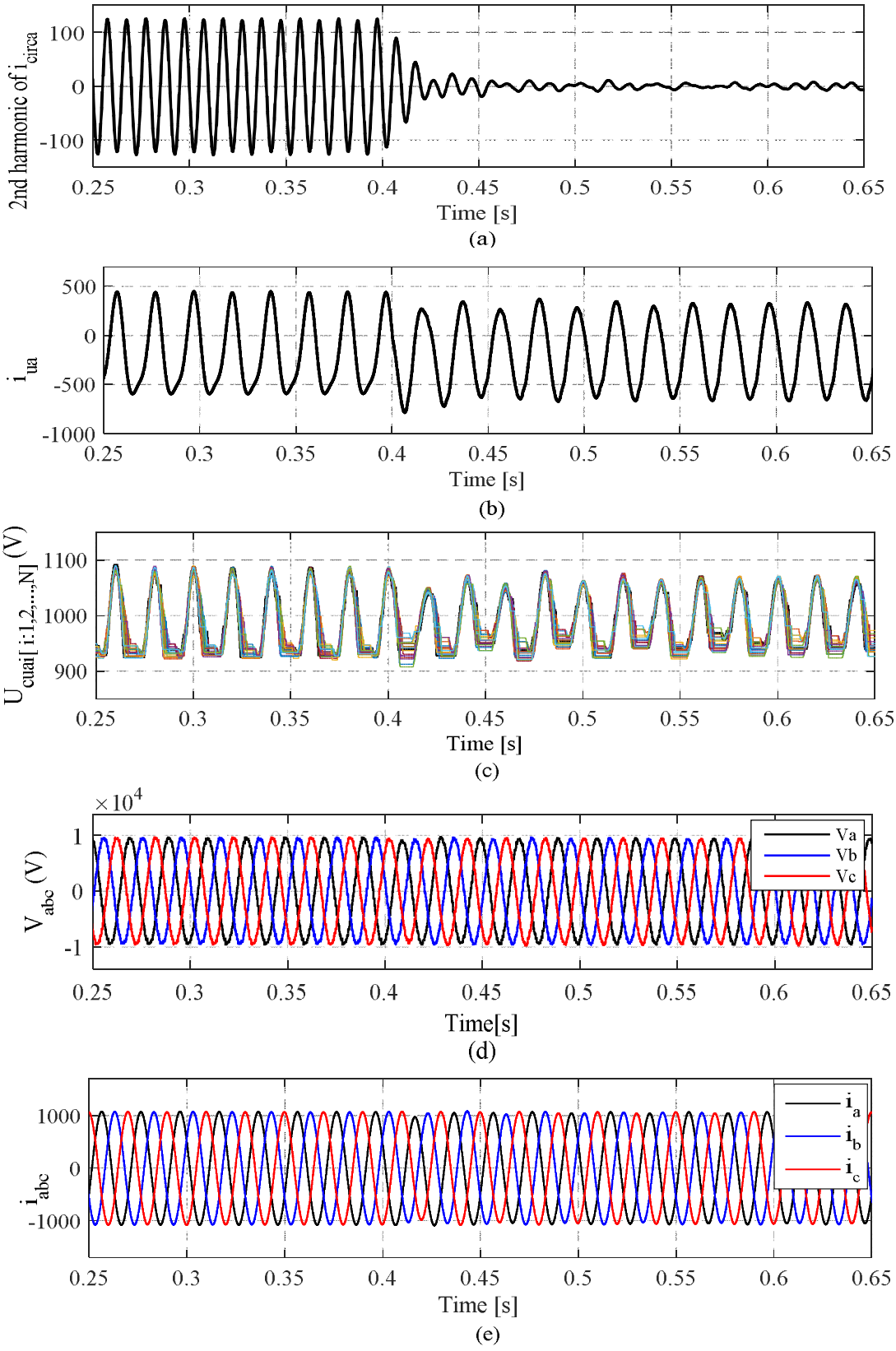

Fig. 7. Simulated waveforms of the MMC using circulating current control:
(a) second harmonic component of the circulating current, (b)upper arm current of phase-a, (c) upper arm SM capacitor voltages of phase-a, (d) output voltages of MMC, and (e) output currents of MMC.

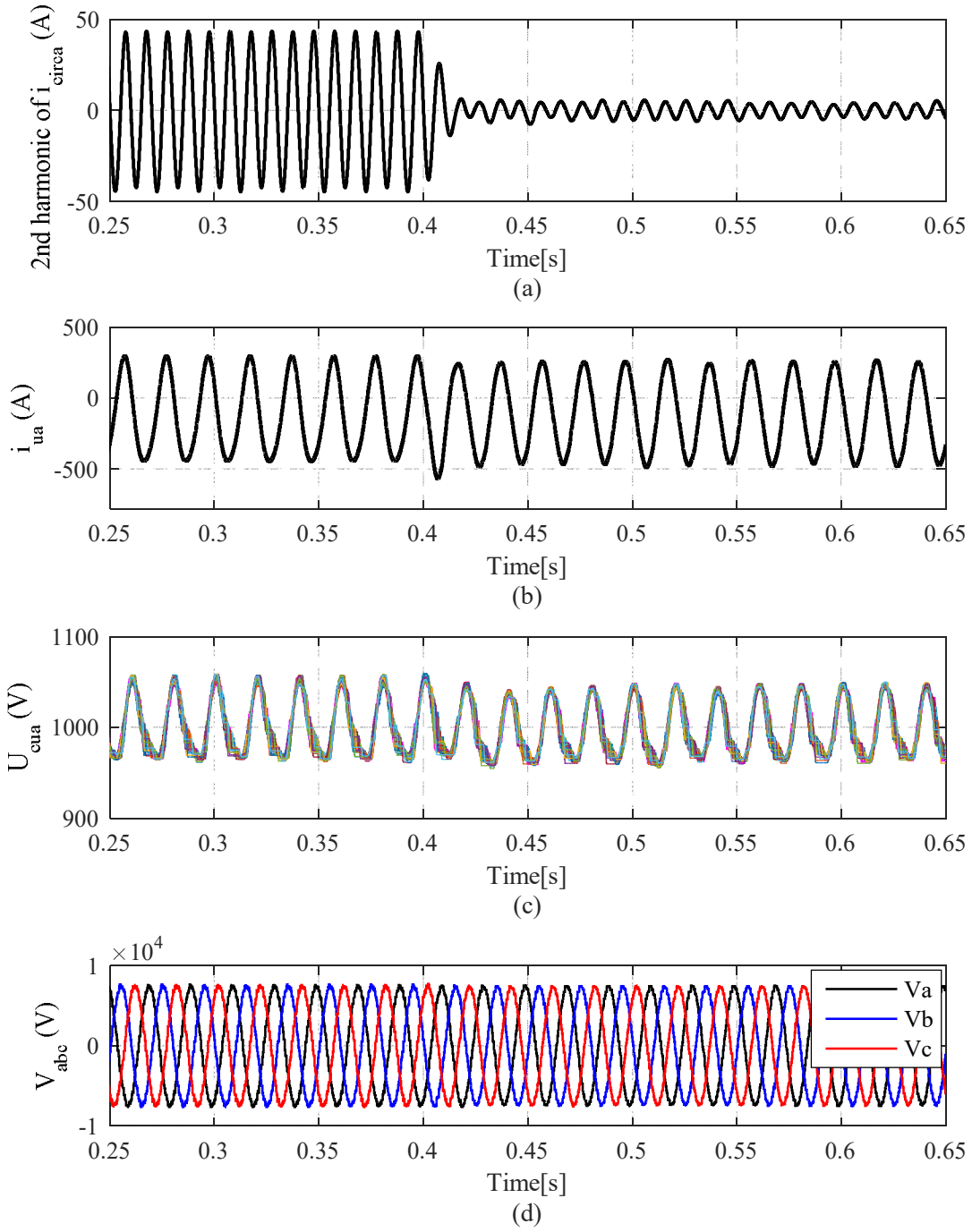

Fig. 8. Simulated waveforms of the MMC with 20% increase in all L_{arm}, L_c, and C component values: (a) second harmonic component of the circulating current, (b)upper arm current of phase-a, (c) upper arm SM capacitor voltages of phase-a, and (d) output voltages of MMC.

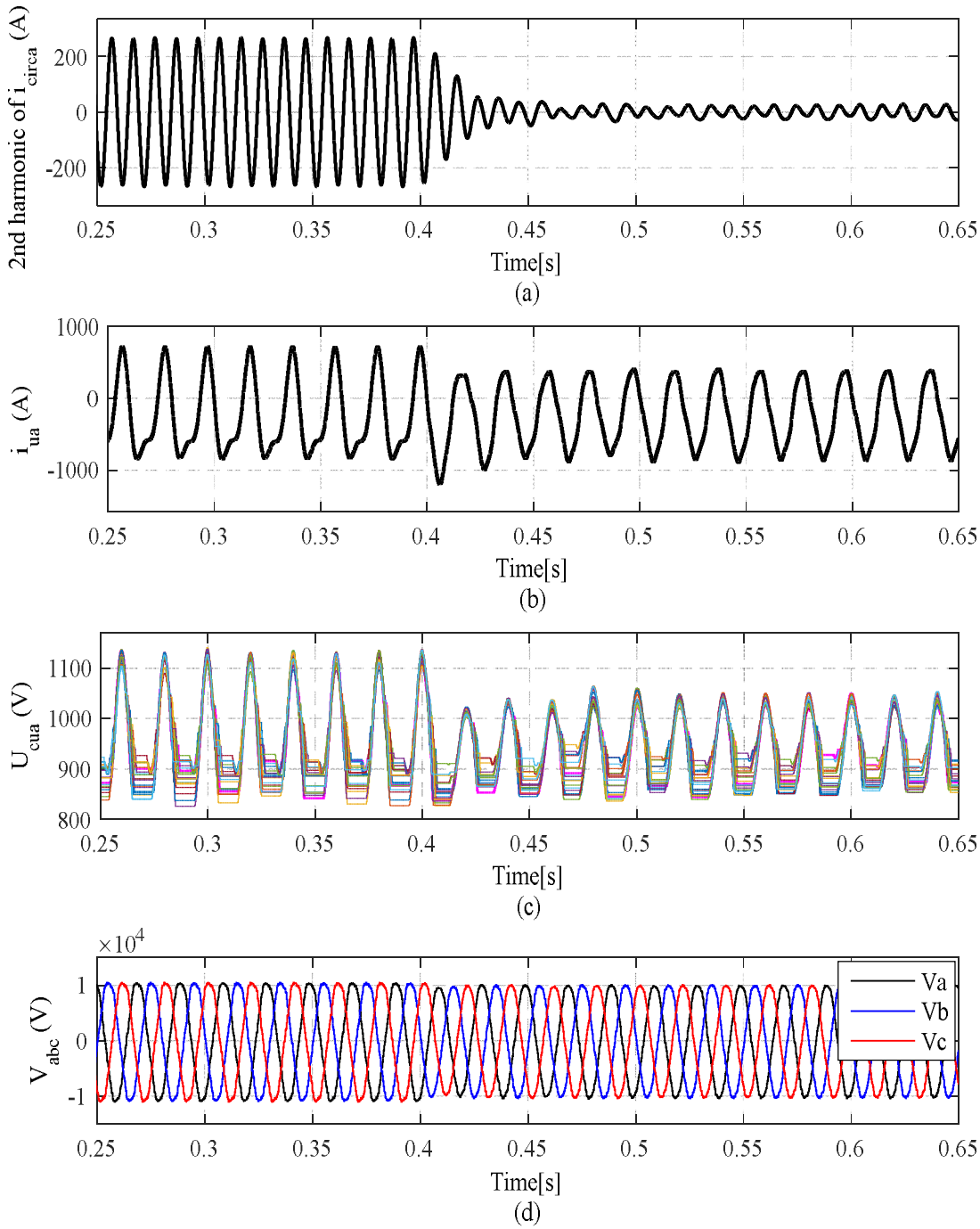

Fig. 9. Simulated waveforms of the MMC with 20% decrease in all L_{arm}, L_c, and C component values: (a) second harmonic component of the circulating current, (b)upper arm current of phase-a, (c) upper arm SM capacitor voltages of phase-a, and (d) output voltages of MMC.

On the other hand, circulating current control has also been evaluated based on the second harmonic dynamics of MMC (presented in equation (35) of the manuscript). As it can be seen, circulating current can be affected by either L_{arm} or U_{cu}^{Σ} variations while the latter depends on SM capacitor values. In this regard, the operation of the proposed controller has been evaluated, applying ±%20 changes in L_{arm} values and the results are demonstrated in Fig. 10(b) and Fig. 10(c) respectively. It can be seen that the proposed controller is capable of eliminating the second harmonic components of current in both scenarios. Moreover, the controller has also been evaluated, applying ±%20 changes in C_{SM} values and the results are demonstrated in Fig. 10(d) and Fig. 10(e) respectively. Simulation results show that the controller is capable of providing an effective reduction in second harmonic components of circulating currents in either case.

Also, the proposed controller is capable of providing specified values of active and reactive power within the maximum stable operation range. As it can be seen in Fig. 11, the output active and reactive power signals of the converter are perfectly following the specified reference values.

5. Conclusion

In this paper, an innovative control method has been presented for MMC as an interface between renewable energy sources and the grid. Dynamic and steady state analysis of the proposed model were provided through dc, 1st and 2nd harmonic models of the converter in dq frame. Converter modulation was performed based on the proposed integrated dynamic model. Providing accurate modulation indices relevant to network parameters and converter parameters was the first novel contribution of the proposed control method over other control techniques. Following the addition of capacitor voltage balancing algorithm, the functionality of the proposed controller was verified by rigorous simulations in MATLAB/Simulink. On the other hand, converter's stable operation range has been developed based on the equations of transferred power. In order to achieve a stable performance, circulating current control has been designed based on second harmonic dynamics of the proposed model, which was considered as the second novel contribution of the proposed control method. It has been shown that by adding specific components to the prior modulation indices, the second harmonic component of the circulating currents can be effectively reduced. Therefore, the harmonic losses were declined while arm currents of each phase became more sinusoidal. As clearly verified in this paper, this operation strategy based on the proposed control method decreased capacitor voltage fluctuations, resulting in an enhanced output quality.

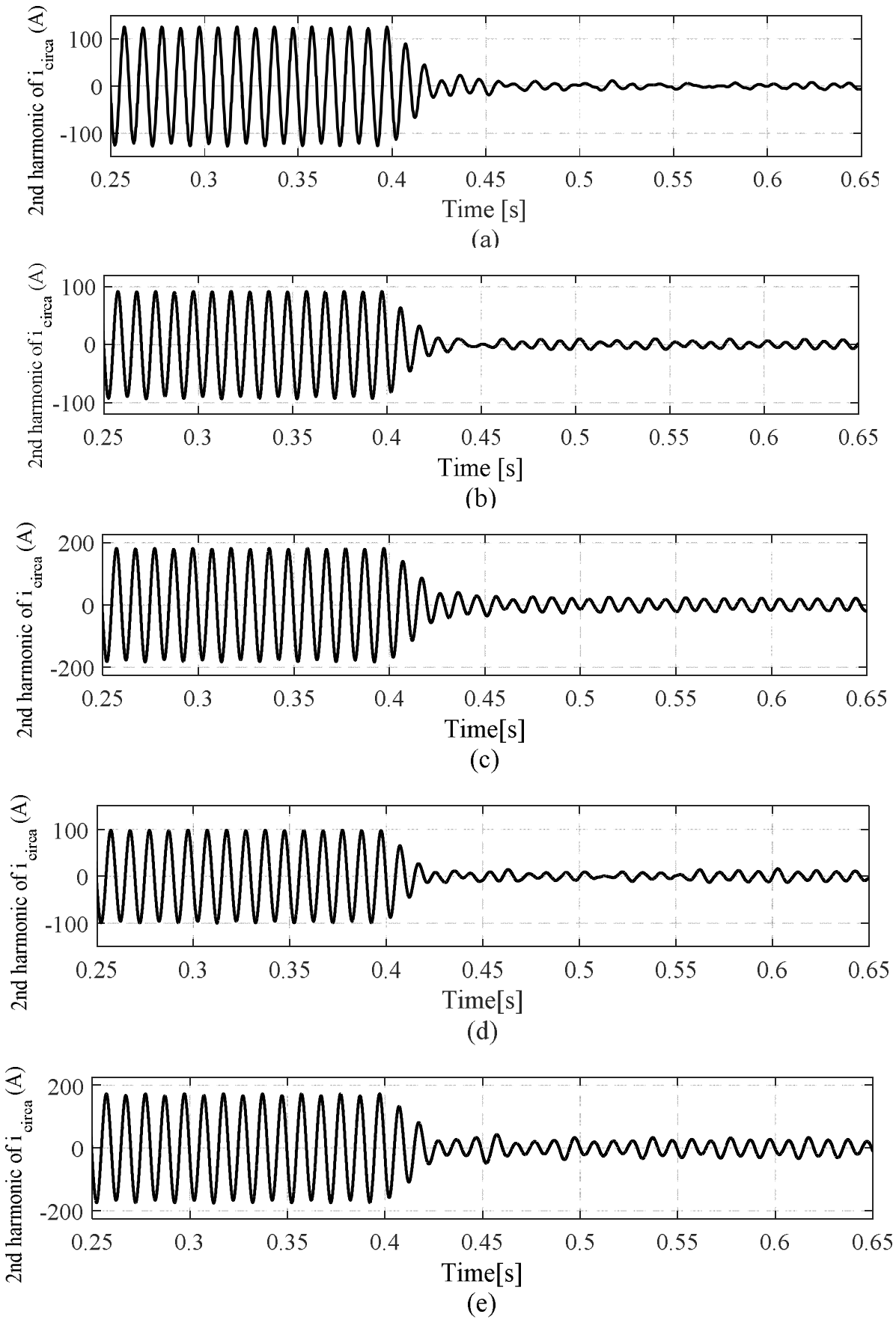

Fig. 10. Simulation results for second harmonic component of i_{circa}, (a) L_{arm}=9mH and C_{SM}=10mF, (b) L_{arm}=1.2×9mH and C_{SM}=10mF, (c) L_{arm}=0.8×9mH and C_{SM}=10mF, (d) L_{arm}=9mH and C_{SM}=1.2×10mF, (e) L_{arm}=9mH and C_{SM}=0.8×10mF.

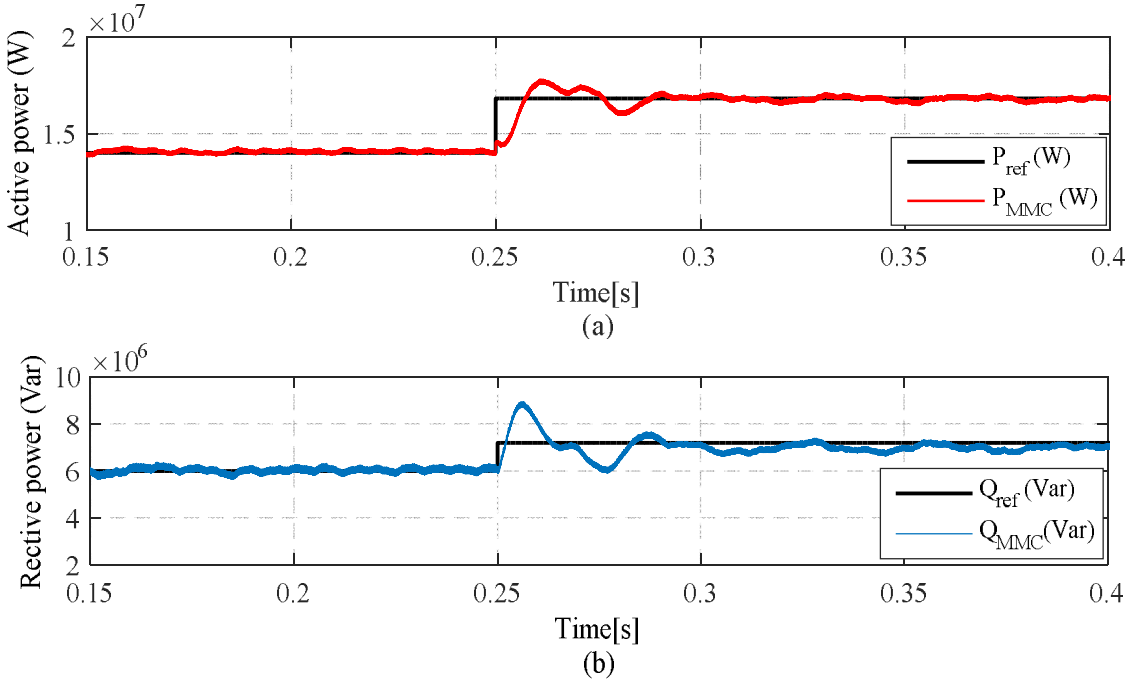

Fig. 11. Simulation results for power components exchanged with the grid, (a) active power of the converter, (b) reactive power of the converter.

6. Appendix

Two nonspecific signals *X(t)* and *Y(t)*, are considered including zero sequence, fundamental and second harmonic components as:

$$X(t) = X_0 + X_D \cos\omega t + X_Q \sin\omega t + X_{D2} \cos 2\omega t + X_{Q2} \sin 2\omega t$$

$$Y(t) = Y_0 + Y_D \cos\omega t + Y_Q \sin\omega t + Y_{D2} \cos 2\omega t + Y_{Q2} \sin 2\omega t$$

By expanding the abc frame form and neglecting 3rd and 4th harmonic components, the product signal *Z(t)=X(t).Y(t)* will be obtained for zero sequence, fundamental frequency and second harmonic as follows:

$$Z(t) = \underbrace{\left(X_0 Y_0 + \frac{X_D Y_D}{2} + \frac{X_Q Y_Q}{2} + \frac{X_{D2} Y_{D2}}{2} + \frac{X_{Q2} Y_{Q2}}{2} \right)}_{Z_0}$$

$$+ \underbrace{\left(X_D Y_0 + X_0 Y_D + \frac{X_{D2} Y_D}{2} + \frac{X_{Q2} Y_Q}{2} + \frac{X_D Y_{D2}}{2} + \frac{X_Q Y_{Q2}}{2} \right)}_{Z_d} \cos\omega t + \underbrace{\left(X_Q Y_0 + X_0 Y_Q - \frac{X_{D2} Y_Q}{2} + \frac{X_{Q2} Y_D}{2} - \frac{X_Q Y_{D2}}{2} + \frac{X_D Y_{Q2}}{2} \right)}_{Z_q} \sin\omega t$$

$$+ \underbrace{\left(\frac{X_D Y_D}{2} - \frac{X_Q Y_Q}{2} + X_{D2} Y_0 + Y_{D2} X_0 \right)}_{Z_{d2}} \cos 2\omega t + \underbrace{\left(\frac{X_Q Y_D}{2} + \frac{X_D Y_Q}{2} + X_{Q2} Y_0 + Y_{Q2} X_0 \right)}_{Z_{q2}} \sin 2\omega t$$

Acknowledgment

This work was supported by FEDER funds through COMPETE 2020 and by Portuguese funds through FCT, under Projects SAICT-PAC/0004/2015 - POCI-01-0145-FEDER-016434, POCI-01-0145-FEDER-006961, UID/EEA/50014/2013, UID/CEC/50021/2013, UID/EMS/00151/2013, and SFRH/BPD/102744/2014. Also, the research leading to these results has received funding from the EU Seventh Framework Programme FP7/2007-2013 under grant agreement no. 309048..

References

[1] Wang M, Hu Y, Zhao W, Wang Y, Chen G. Application of modular multilevel converter in medium voltage high power permanent magnet synchronous generator wind energy conversion systems. IET Renewable Power Generation 2016; 10: 824- 833.

[2] Kim J. C., Cho S. M., and Shin H. S. Advanced power distribution system configuration for smart grid. *IEEE Trans. Smart Grid* 2013; 4:353-358.

[3] Zhang X. P., Rehtanz C., and Pal B. Flexible AC Transmission Systems: Modeling and Control. Springer; 2012.

[4] Debnath S., Qin J., Bahrani B., Saeedifard M., and Barbosa P. Operation, control, and applications of the modular multilevel converter: a review. IEEE Trans. Power electronics 2015; 30:37-53.

[5] Nami A., Liang J., Dijkhuizen F., and Demetriades G. D. Modular multilevel converters for HVDC applications: review on converter cells and functionalities. IEEE Trans. Power Electronics 2015; 30:18-36.

[6] Chang Y, Shi G, Zhang J, Cai X. Analysis and design of a MMC based wind power converter for offshore dc grids. IEEE Industrial Electronics Society Conference (IECON) 2015: 1363- 1368.

[7] Sahoo A K, Otero-De-Leon R, Mohan N. Review of modular multilevel converters for teaching a graduate-level course of power electronics in power systems. In North American Power Symposium, 2013: 1-6.

[8] Perez M A, Bernet S, Rodriguez J, Kouro S, Lizana R. Circuit topologies, modelling, control schemes and applications of modular multilevel converters. IEEE Trans Power Elects 2015; 30: 4-17.

[9] Debnath S, Saeedifard M. A new hybrid modular multilevel converter for grid connection of large wind turbines. IEEE Trans. Sustainable Energy 2013; 4: 1051-1064.

[10] Franquelo L.G., Rodriguez J., Leon J. I., Kouro S., Portillo R., Prats M. A. M. The age of multilevel converters arrives. IEEE Industrial Electronics Magazine 2008; 2: 28-39.

[11] Lesnicar A, Marquardt R. An innovative modular multilevel converter topology suitable for a wide power range. In IEEE Bologna Power Tech conference,2003: 1-6.

[12] Mehrasa M, Pouresmaeil E, Zabihi S, Catalao J. P. S. Dynamic Model, Control and Stability Analysis of MMC in HVDC Transmission Systems. IEEE Trans. on Power Delivery 2017; 32: 1471-1482.

[13] Mehrasa M, Pouresmaeil E, Zabihi S, Vechiu I, Catalao J. P. S. A multi-loop control technique for the stable operation of modular multilevel converters in HVDC transmission systems. International Journal of Electrical Power & Energy Systems 2018; 96: 194 -207.

[14] Antonopoulos A, Angquist L, Norrga S, Ilves K, Nee H P. Modular multilevel converter AC motor drives with constant torque from zero to nominal speed. IEEE Energy Convers. Congr. 2012: 739–746.

[15] Debnath S, Qin J, Saeedifard M. A distributed PWM strategy for modular multilevel converter. IEEE Industrial Electronics Society conference 2014: 1014 – 1020.

[16] Saeedifard M, Nikkhajoei H, Iravani R, Bakhshai A. A space vector modulation approach for a multimodule HVDC converter system. IEEE Trans. Power Delivery 2007; 22: 1643– 1654.

[17] Ahmad Khan N, Vanfretti L, Li W,Haider A. Hybrid nearest level and open loop control of modular multilevel converters. 16th European Conference on Power Electronics and Applications 2014: 1-12.

[18] Hassanpoor A, Norrga S, Nee H, Angquist L. Evaluation of different carrier-based pwm methods for modular multilevel converters for HVDC application. IEEE Industrial Elects Society conference 2012: 388-393.
[19] Angquist L, Antonopoulos A, Siemaszko D,Ilves K, Vasiladiotis M, Nee H. Open-loop control of modular multilevel converters using estimation of stored energy. IEEE Trans. Industry Applications 2011; 47: 2516- 2524.
[20] Siemaszko D, Antonopoulos A, Ilves K, Vasiladiotis M, Ängquist L, Nee H. Evaluation of control and modulation methods for modular multilevel converters. International Power Electronics Conference 2010: 746 – 753.
[21] Hassanpoor A, Norrga S, Nami A. Loss evaluation for modular multilevel converters with different switching strategies. Power Electronics and ECCE Asia Int. conference 2015: 1558 – 1563.
[22] Qin J, Saeedifard M. Reduced switching-frequency voltage-balancing strategies for modular multilevel HVDC converters. IEEE Trans. Power Delivery 2013; 28: 2403 – 2410.
[23] Bahrani B, Debnath S, Saeedifard M. Circulating current suppression of the modular multilevel converter in a double-frequency rotating reference frame. IEEE Trans. Power Electronics 2015; 31: 783-792.
[24] Ilves K, Antonopoulos A, Norrga S, Angquist L, Nee H. Controlling the AC-side voltage waveform in a modular multilevel converter with low energy-storage capability. Power Electronics and Applications European Conference 2011: 1- 8.
[25] Mehrasa M, Pouresmaeil E, Zabihi S, Trujillo Caballero JC,Catalao J. P. S. A Novel Modulation Function-based Control of Modular Multilevel Converters for High Voltage Direct Current Transmission Systems. Energies 2016; 9: 1-14.
[26] Ilves K, Norrga S, Harnefors L, Nee H. On energy storage requirements in modular multilevel converters. IEEE Trans. Power Elects 2013; 29: 77-88.
[27] Harnefors L, Antonopoulos A, Norrga S, Ängquist L, Nee H. Dynamic analysis of modular multilevel converters. IEEE Trans. Industrial Elects 2013; 60: 2526 – 2537.
[28] Norrga S, Ängquist L, Ilves K, Harnefors L, Nee H. Decoupled steady-state model of the modular multilevel converter with half-bridge cells. IET International Conference on Power Electronics, Machines and Drives(PEMD) 2012: 1-6.
[29] Mehrasa M, Pouresmaeil E, Akorede M. F., Zabihi S, Catalao J. P. S. Function-Based Modulation Control for Modular Multilevel Converter under Varying Loading and Parameters Conditions. IET Generation, Transmission & Distribution 2017; 11: 3222-3230.
[30] Mehrasa M, Pouresmaeil E, Taheri S, Vechiu I, Catalao J. P. S. Novel Control Strategy for Modular Multilevel Converters Based on Differential Flatness Theory. IEEE Journal of Emerging and Selected Topics in Power Electronics 2017; DOI: 10.1109/JESTPE.2017.2766047.
[31] Jovcic D, Jamshidifar A. Phasor model of modular multilevel converter with circulating current suppression control. IEEE Trans. Power Deliv. 2014; 30: 1889 – 1897.
[32] Tu, Q., Xu, Z., Xu, L. Reduced switching-frequency modulation and circulating current suppression for modular multilevel converters. IEEE Trans. Power Deliv. 2011; 26: 2009-2017.